

How Bound and Free Fatty Acids in Cellulose Films Impact Nonspecific Protein Adsorption

*Katrin Niegelhell^a, Michael Süßenbacher^b, Jürgen Sattelkow^c, Harald Plank^c, Yonggui Wang^d,
Kai Zhang^d and Stefan Spirk^{a*}*

^aGraz University of Technology, Institute for Paper, Pulp and Fiber Technology, Inffeldgasse 23,
8010 Graz, Austria.

^bGraz University of Technology, Institute for Chemistry and Technology of Materials,
Stremayrgasse 9, 8010 Graz, Austria.

^cGraz University of Technology, Institute for Electron Microscopy and Nanoanalysis,
Steyrergasse 17, 8010 Graz, Austria.

^dGeorg-August-University of Goettingen, Wood Technology and Wood Chemistry, Büsgenweg
4, 37077 Göttingen, Germany.

Corresponding Author

*E-mail: stefan.spirk@tugraz.at, Phone: +43-316-873-32284

ABSTRACT

The effect of fatty acids and fatty acid esters to impair nonspecific protein adsorption on cellulose thin films is investigated. Thin films are prepared by blending trimethylsilyl cellulose solutions with either cellulose stearoyl ester or stearic acid at various ratios. After film formation by spin coating, the trimethylsilyl cellulose fraction of the films is converted to cellulose by exposure to HCl vapors. The morphologies and surface roughness of the blends were examined by atomic force microscopy revealing different feature shapes and sizes depending on the blend ratios. Nonspecific protein adsorption at the example of *bovine serum albumin* towards the blend thin films was tested by means of surface plasmon resonance spectroscopy in real-time. Incorporation of stearic acid into the cellulose leads to highly protein repellent surfaces regardless of the amount added. The stearic acid acts as a sacrificial compound that builds a complex with *bovine serum albumin* thereby inhibiting protein adsorption. For the blends where stearoyl ester is added to the cellulose films, the cellulose:cellulose stearoyl ester ratios of 3:1 and 1:1 lead to much lower nonspecific protein adsorption compared to pure cellulose, whereas for the other ratios, adsorption increases. Supplementary results were obtained from atomic force microscopy experiments performed in liquid during exposure to protein solution and surface free energy determinations.

KEYWORDS

Cellulose thin film; stearic acid; cellulose stearoyl ester; protein adsorption; surface plasmon resonance; blend

INTRODUCTION

Fatty acids and their esters represent important biomolecules since they are involved in many biochemical processes. One of their main functions is their involvement in energy storage by formation of mono-, di- and triglycerides in animals and plants. However, there are innumerable biochemical pathways where fatty acid (esters) are involved or even act as co-enzymes such as lipoic acid for instance.¹ Their high abundance in nature makes fatty acids and their esters inexpensive raw materials, which are currently used in a variety of areas. For instance, they are used in food industry as emulsifying, release or glazing agents due to their amphiphilic character. Actually, sodium or potassium salts of fatty acids are able to act as efficient soaps or surfactants.^{2, 3} Fatty acid esters of biopolymers have attracted significant interest in the past years, since they are easy to manufacture (e.g. by reaction with fatty acid chlorides in the presence of a base), cheap and widely accessible.⁴⁻⁷ A particularly interesting field of research was opened by the investigation of cellulose fatty acid esters either as bulk or nanomaterials such as cellulose nanocrystals and nanofibrils.⁸⁻¹⁵ The usual fields of application for cellulose fatty acid ester products are food, paper or textile industry and packaging.¹⁶ Therefore, cellulose fatty acid ester materials are tested predominantly for properties concerning such applications, e.g. water and oxygen barrier properties, processability and mechanical properties.^{12, 17-21} However, in life science applications they have gained less attraction. In these applications, very often a detailed investigation of surface properties is a major issue, e.g. the interaction capacity with proteins or living cells. Adsorbed protein layers can lead to the adhesion of particles, bacteria and cells, which is inadvertent when it comes to the promotion of inflammation²² or fouling processes.²³ Nevertheless, proteins present on a surface can act advantageously as well, for instance, they mediate vascularization in artificial tissue scaffolds²⁴ or enable the deposition of

certain cells²⁵ or other compounds, such as gold nanoparticles.²⁶ However, for biopolymer blend thin films just little data is available on the interaction with proteins^{27, 28} and for blend thin films involving cellulose and fatty acids or esters thereof there is not any data available to the best of our knowledge.

Our starting point in this research was how the presence of fatty acids impacts nonspecific protein adsorption. As model systems, blend films were chosen which contain cellulose and stearic acid (SA) and, for the sake of comparison, cellulose that contains stearylated cellulose. Various ratios of the blend films have been prepared and after thorough characterization of the surface properties, their interaction behavior with proteins was tested by surface resonance plasmon spectroscopy at low protein concentration ($1 \text{ mg}\cdot\text{ml}^{-1}$ BSA) as well as high concentrations ($50 \text{ mg}\cdot\text{ml}^{-1}$ BSA) which are usually present in blood plasma. The ratios were chosen in a way that we have different scenarios: CSE in a cellulose phase, a bicontinuous phase, and cellulose in a CSE phase.

MATERIALS AND METHODS

Materials. Trimethylsilyl cellulose (Avicel, $M_w = 185,000 \text{ g}\cdot\text{mol}^{-1}$, $M_n = 30,400 \text{ g}\cdot\text{mol}^{-1}$, PDI = 6.1 determined by GPC in chloroform) with a DS_{Si} value of 2.8 was purchased from TITK (Rudolstadt, Germany). Chloroform (99.3%), disodium phosphate heptahydrate ($\text{Na}_2\text{HPO}_4\cdot 7\text{H}_2\text{O}$), sodium dihydrogen phosphate monohydrate ($\text{NaH}_2\text{PO}_4\cdot\text{H}_2\text{O}$), hydrochloric acid (37%), sodium chloride (Ph.Eur.), sodium hydroxide (99%), *bovine serum albumin* (lyophilized powder, $\geq 96\%$, 66.5 kDa) and stearic acid ($\geq 95\%$) were bought from Sigma Aldrich and used without further purification. Cellulose stearyl ester (CSE, $DP_w = 430$, $DP_n = 210$) with the degree of substitution of 3 was prepared according to a literature procedure.²⁹ SPR gold sensor slides

(CEN102AU) were purchased from Cenibra, Germany. Milli-Q water (resistivity = 18.2 M Ω ·cm) from a Millipore water purification system (Millipore, USA) was used for contact angle measurements and buffer preparation.

Substrate Cleaning and Film Preparation. SPR gold sensor slides/silicon wafers were immersed in caro's acid (H₂O₂ (30 wt.%)/H₂SO₄ (1:3 v/v)) for 10 min and subsequently rinsed extensively with Milli-Q water followed by drying in a stream of nitrogen gas. Trimethylsilyl cellulose, cellulose stearoyl ester and stearic acid were dissolved in chloroform (0.75 wt.%) by stirring over night at room temperature and filtered through 0.45 μ m PVDF filters. The solutions were spin coated either pure or in ratios of 3:1, 1:1 and 1:3 for TMSC:SA and TMSC:CSE by depositing 120 μ l solution onto the cleaned substrate and rotating at a spinning speed of 4000 rpm and an acceleration of 2500 rpm·s⁻¹ for a period of 60 s. The regeneration of trimethylsilyl cellulose to cellulose was done by treatment with acidic vapors. The substrates were placed in a petri-dish (\varnothing 5 cm) next to 3 ml of 10 wt.% hydrochloric acid. Then the dish was closed with its cap and the films were exposed to the acidic atmosphere for 15 min. The conversion was confirmed by ATR-IR spectroscopy and water contact angle measurements as reported elsewhere.^{30, 31}

Buffer and Protein Solution Preparation. In all experiments, a 10 mM phosphate buffer with ionic strength of 100 mM sodium chloride was used. Buffer salts (Na₂HPO₄·7H₂O and NaH₂PO₄·H₂O) were dissolved in Milli-Q water and the pH value of the solution was adjusted to a value of 7.4 by adding 0.1 M sodium hydroxide. *Bovine serum albumin* was dissolved in the buffer at a concentration of 1 mg·ml⁻¹ and 50 mg·ml⁻¹.

Infrared Spectroscopy. ATR-IR spectra were recorded on an ALPHA FT-IR spectrometer (Bruker, Billerica, MA, USA) using a PLATINUM attenuated total reflection (ATR) single

reflection diamond ATR module. Spectra were attained in a scan range between 4000 to 400 cm^{-1} with 48 scans and a resolution of 4 cm^{-1} . The data was analyzed with OPUS 4.0 software.

Stylus Profilometry. Film thicknesses were measured with a DETAK 150 Stylus Profiler from Veeco. Measurements were performed with a scan length of 1000 μm and a force of 3 mg over a duration of 3 seconds. The resolution and measurement range were 0.333 μm per sample and 6.5 μm , respectively. A diamond stylus with a radius of 12.5 μm was applied. Samples were measured after scratching the film (deposited on a silicon wafer). The resulting profile was used to calculate the thickness of different films. All measurements were performed at least three times.

Contact Angle (CA) and Surface Free Energy (SFE) Determination. Static contact angle measurements were performed with a Drop Shape Analysis System DSA100 (Krüss GmbH, Hamburg, Germany) with a T1E CCD video camera (25 fps) and the DSA1 v 1.90 software. Measurements were conducted with Milli-Q water and di-iodomethane using a droplet size of 3 μl and a dispense rate of 400 $\mu\text{l}\cdot\text{min}^{-1}$. All measurements were performed at least three times. CA were calculated with the Young-Laplace equation and SFE was determined with the Owen-Wendt-Rabel-Kaelble (OWRK) method.³²⁻³⁴ It should be mentioned here that the determination of the SFE by wettability measurements is – although very informative – an indirect method. Therefore, potential influences of surface roughness and film characteristics may influence the value of the SFE to a certain extent.

Atomic Force Microscopy – AFM. AFM images were attained in tapping mode in ambient atmosphere at room temperature by a Veeco Multimode QuadraX MM scanning probe microscope (Bruker, Billerica, MA, USA) using Si-cantilevers (NCH-VS1-W from NanoWorld AG, Neuchatel, Switzerland) with a resonance frequency of 320 kHz and a force constant of 42

$\text{N}\cdot\text{m}^{-1}$. Root mean square (RMS) roughness calculation and image processing was performed with the Nanoscope software (V7.30r1sr3, Veeco). AFM investigations of the films in liquid were performed with a Fast Scan Bio atomic force microscope (Bruker AXS, Santa Barbara, CA, USA) operated by a Nanoscope V controller. All experiments were conducted in a droplet of buffer solution liquid by using Fast Scan D cantilevers with a resonance frequency of 110 kHz and a force constant of $0.25 \text{ N}\cdot\text{m}^{-1}$. The samples were measured at air as a reference. Image recording in liquid was done after equilibration of the samples for 30 min in buffer and after treatment with protein solution and subsequent rinsing with buffer. Set points, scan rates and controlling parameters were chosen carefully to ensure lowest possible energy dissipation to the sample and to exclude tip driven artifacts. Data analysis of the images was performed using Nanoscope Analysis 1.50 (Build R2.103555, Bruker AXS, Santa Barbara, CA, U.S.A.) and Gwyddion 2.38.

Multi Parameter Surface Plasmon Resonance Spectroscopy – MP-SPR. MP-SPR studies were performed with a MP-SPR NaviTM 210A VASA (Bionavis Ltd., Tampere, Finland) equipped with two lasers ($\lambda = 670 \text{ nm}, 785 \text{ nm}$) in both measurement chambers, using gold coated SPR sensor slides (gold layer 50 nm, chromium adhesion layer 10 nm). All measurements were carried out using a full angular scan ($39\text{--}78^\circ$, scan speed: $8^\circ\cdot\text{s}^{-1}$). The MP-SPR experiments were conducted in the following way. The equilibration of the samples coated onto the sensor slides was done by rinsing with Milli-Q water followed by buffer. After a steady signal was observed, protein solution was injected into the flow cell and pumped through at a flow of $50 \mu\text{l}\cdot\text{min}^{-1}$ for a duration of 5 min. The samples were rinsed with buffer again followed by Milli-Q water and dried in a stream of N_2 gas. All experiments were performed in three parallels.

Protein adsorption was quantified according to equation 1, which considers the dependence of the angular response $\Delta\theta$ of the surface plasmon resonance in dependence of the refractive index increment (dn/dc) of the adsorbing layer.³⁵

$$\Gamma = \frac{\Delta\theta \times k \times d_p}{dn/dc} \quad (1)$$

For thin layers (<100 nm), $k \times d_p$ can be considered constant and can be obtained by calibration of the instrument by determination of the decay wavelength l_d . For the MP-SPR Navi™ 210 A VASA used in this study, $k \times d_p$ values are approximately $1.09 \times 10^{-7} \text{ cm}^\circ$ (at 670 nm) and $1.9 \times 10^{-7} \text{ cm}^\circ$ (at 785 nm) in aqueous systems. The dn/dc of proteins in water-based buffer systems was reported to be $0.187 \text{ cm}^3 \cdot \text{g}^{-1}$, which was used to calculate the amount of adsorbed masses.³⁶

RESULTS AND DISCUSSION

Preparation of blend thin films. Blend thin films were prepared by spin coating TMSC and CSE or TMSC and SA mixtures at different ratios. The films were exposed to hydrochloric acid vapors in order to convert TMSC into cellulose to create cellulose/CSE and cellulose/SA blend films. It is important to track changes which occur during the exposure to the HCl vapors. The ATR-IR spectra clearly show that the esters (neither in bulk nor in the film) as well as the fatty acids are not altered by the regeneration procedure (ESI†, Figure S1, S2). Furthermore, the morphology of pure CSE and SA films does not seem to be affected (Fig.1, AFM images). A further indication for the inertness of CSE and SA films towards HCl vapors is the wettability with water and diiodomethane, which does not change after the HCl treatment (†ESI, Figure S3, S4).

Regeneration of TMSC was monitored by ATR-IR spectroscopy (bands attributed to CH_3 of TMSC at 2960 cm^{-1} (ν_{asym}) and 2872 cm^{-1} (ν_{sym}) and Si-C at 1251 cm^{-1} and 842 cm^{-1} disappear, the OH band between 3600 and 3000 cm^{-1} arises), wettability behavior (static water CA change from 94° to 46°) and thickness determination (shrinkage ca. 60%). For the blend films, conversion was confirmed by ATR-IR spectroscopy; the spectra of the 1:1 ratio for both types of blends is depicted in Figure S5 and S6 (†ESI). Surface free energies (SFE) depicted in Figure 2 further corroborate these findings.

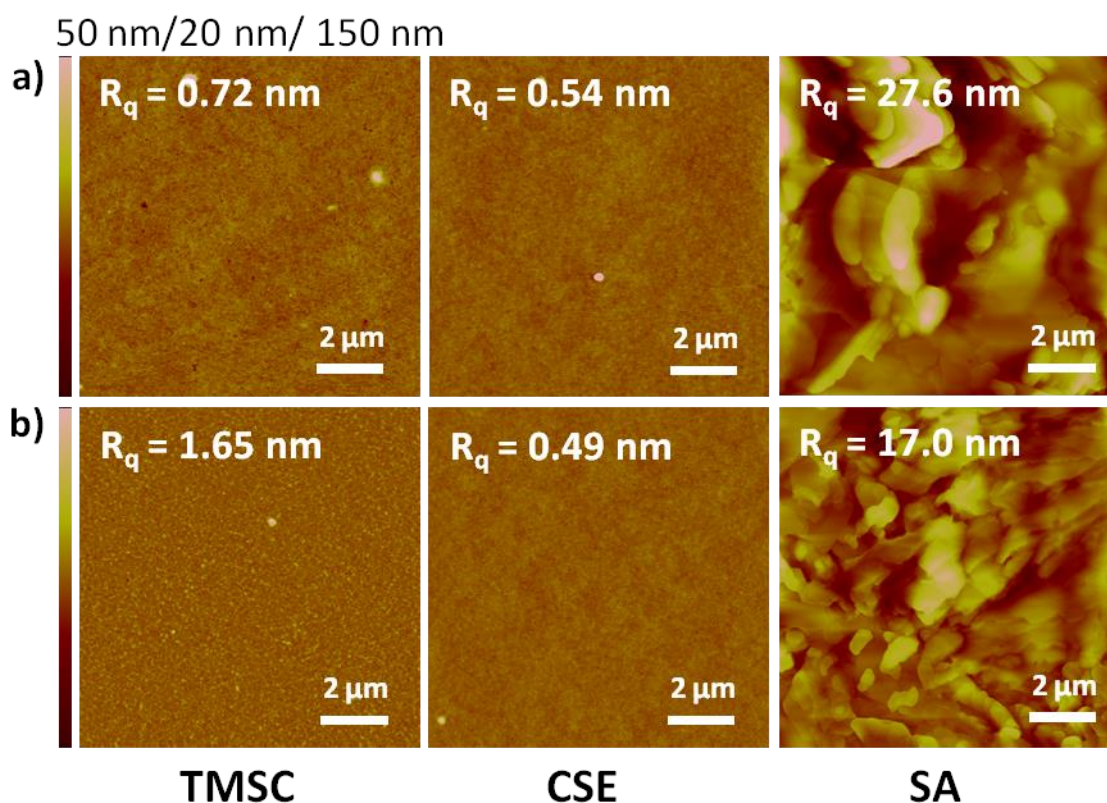


Figure 1. Atomic force microscopy height images and corresponding RMS roughness (R_q) of pure spin coated films before (a) and after (b) treatment with HCl vapors (picture size $10 \times 10\ \mu\text{m}^2$).

The SFE of TMSC changes upon conversion from low to high SFEs and polar contributions to the SFE increase showing the hydrophilic character of cellulose. SFEs of CSE and SA remain constant, which further substantiates the resistance of the substances to acidic vapor treatment. The blends feature similar SFEs at all ratios, which are closer to the value of CSE and SA before regeneration. After conversion, the SFE increases for all ratios, however, some differences arise.

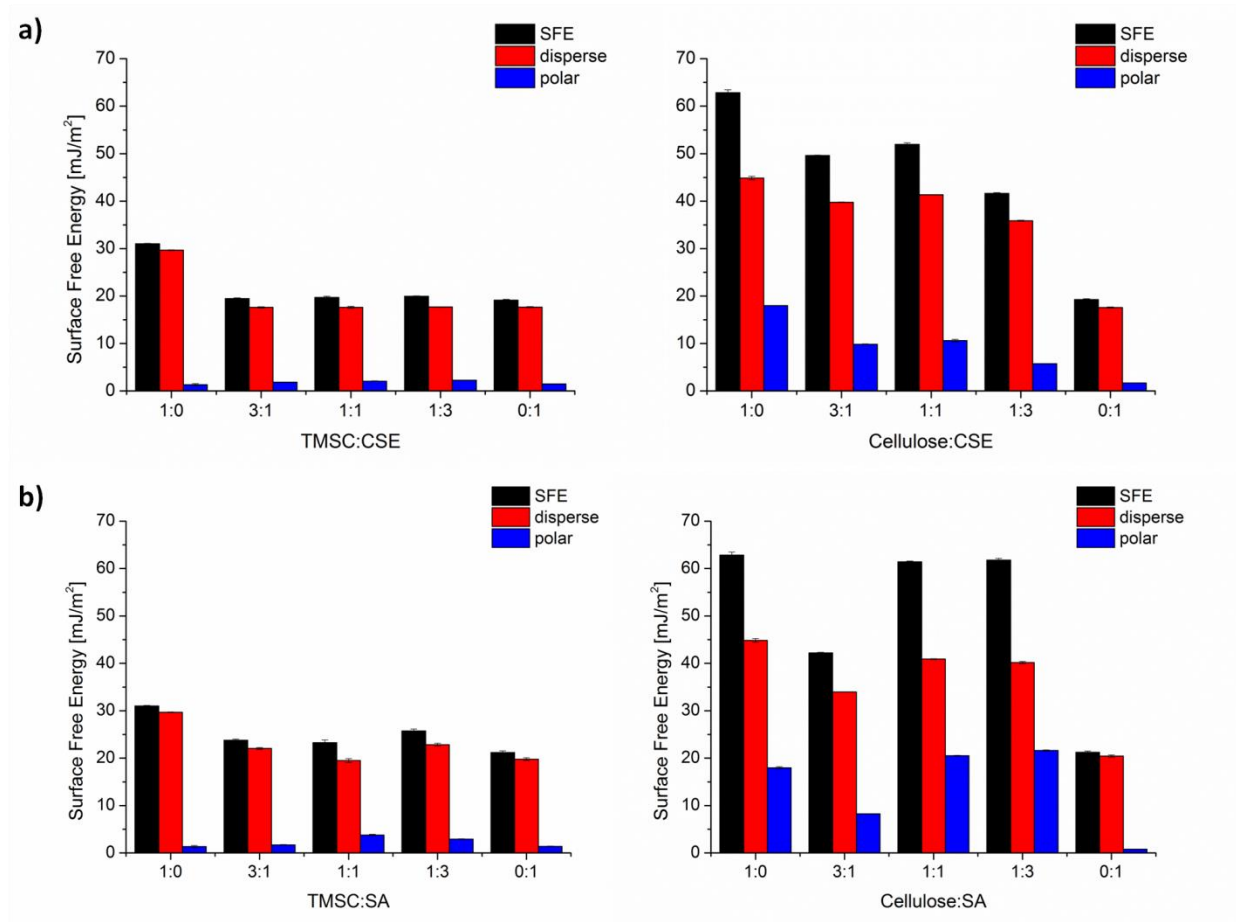


Figure 2. Surface free energies of blend films from TMSC:CSE (a) and TMSC:SA (b) at different ratios before (left) and after (right) regeneration.

Phase separation behavior. The resulting morphologies of the blend thin films were investigated by atomic force microscopy. For the cellulose:CSE blend, microphase separation occurs (Figure 3). The assignment of the resulting phases to the compounds of the blend was

accomplished by evaluation of the shrinkage of the TMSC domains upon conversion, which was 63-68 % for all TMSC domains at all ratios as reported in literature for pure TMSC films.^{30, 37} Additionally, treatment with CHCl_3 of the regenerated films was performed leaving only the cellulose part of the films behind. The cellulose:CSE blend at a ratio of 3:1 forms a continuous TMSC phase containing CSE domains, whereas at the other ratios the inverse morphology is found. Domain sizes of the different blend ratios are summarized in Table 1.

The phase separation behavior of the polymer-polymer blend can be explained by the transient bilayer theory, stating vertical stratification of the two polymer phases, followed by lateral phase separation due to interfacial instabilities caused by the evaporation of solvent and a concomitant solvent-concentration gradient in the film.³⁸ Due to preferential migration to the air-polymer interface of the compound with lower surface free energy, in this case CSE, TMSC forms the layer at the bottom that is in contact with the substrate during the early stages of spin coating. Then, as the solvent proceeds to evaporate, dewetting processes come into play. As for the cellulose:CSE blend at a ratio of 3:1, a thin CSE top layer is present that starts to dewet and contracts into droplets. The emergent voids are then filled with TMSC resulting in a continuous TMSC phase, which contains round CSE domains. Since CSE is the better soluble compound in CHCl_3 , the solvent remains longer in the CSE than in the TMSC phase, leading to a collapse of the CSE phase at the end of the spin coating process.³⁹ The arising CSE droplets therefore migrate into the surrounding, bottom TMSC phase. This effect was previously observed for other binary polymer blends as well.⁴⁰ In the case of the cellulose:CSE blend at a ratio of 1:3, a rather thick CSE layer is present on top of a thin TMSC layer. Dewetting causes this thick layer to break up and generates holes, which are subsequently filled by the polymer from the lower layer favoring the distribution of TMSC inside a continuous CSE phase. The collapse of the better

soluble CSE phase is detected for this blend ratio as well. Table 1 summarizes the domain heights for the cellulose:CSE blends. AFM images of the cellulose:CSE blend at a ratio of 1:1 appear to show the formation of two continuous phases, as expected from literature reports.⁴⁰ Upon regeneration, the TMSC part shrinks, causing a higher surface area of the CSE domains. Treatment of those surfaces with CHCl_3 reveals a morphology which diverges from the expected behavior. Cellulose is distributed in a CSE phase, which is presumably induced by differences in the molar mass of the polymers affecting their mobility.

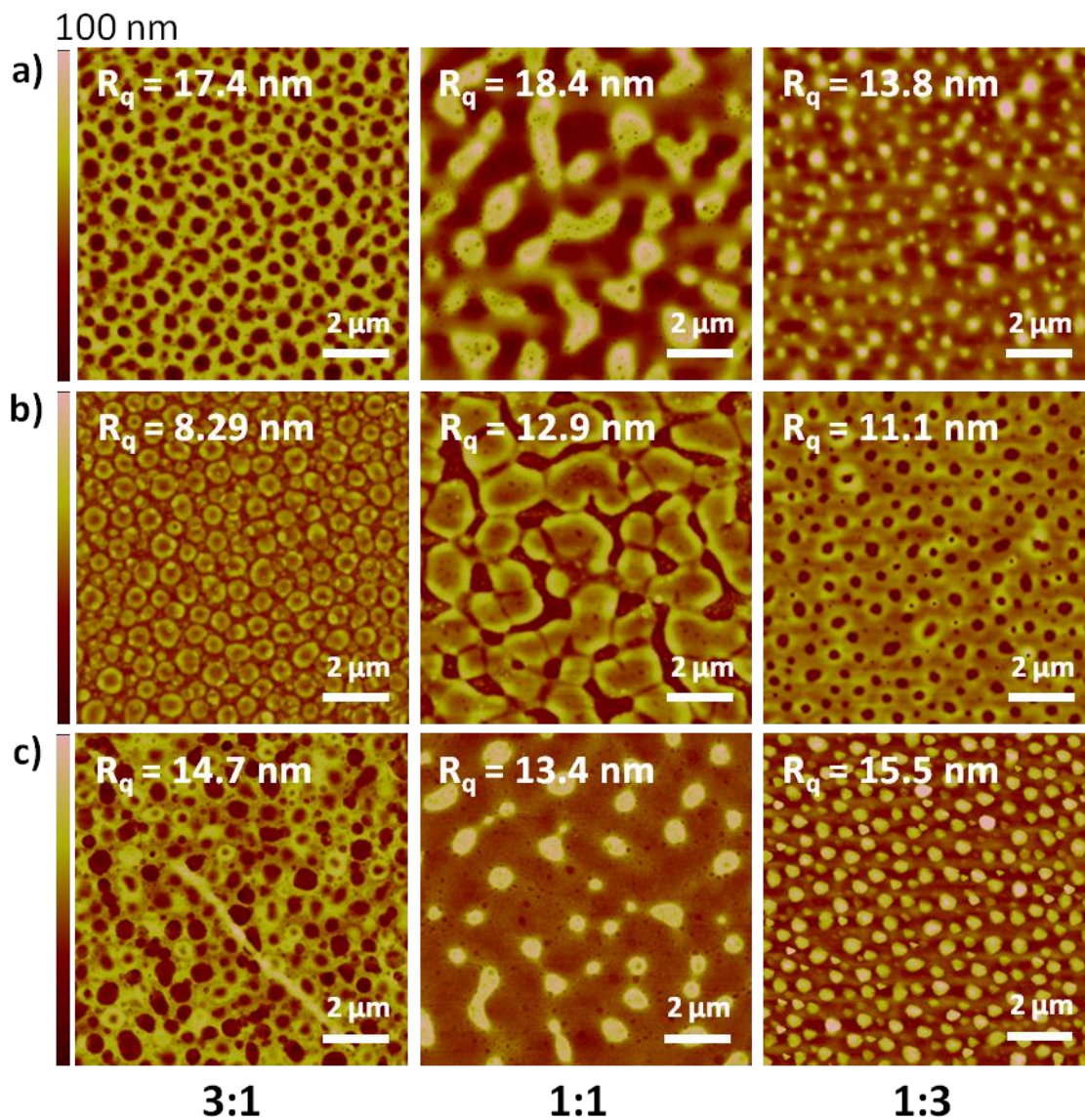


Figure 3. Atomic force microscopy height images and corresponding RMS roughness (R_q) of TMSC:CSE blend films spin coated at different ratios before (a) and after (b) exposure to HCl vapors, as well as after (c) treatment with CHCl_3 (picture size $10 \times 10 \mu\text{m}^2$).

Table 1. Average TMSC and cellulose domain height in respect to CSE for the different blend ratios and average feature sizes of the TMSC/cellulose:CSE blend.

TMSC/cellulose:CSE	3:1 [nm]	1:1 [nm]	1:3 [nm]
TMSC domain height	+ 49 ± 9	+ 47 ± 16	+ 58 ± 22
cellulose domain height	- 24 ± 8	- 42 ± 10	- 35 ± 4
feature size	397 ± 73	773 ± 162	365 ± 110

Although SA is a small molecule, phase separation of the cellulose:SA blend films is observed. SA features a hydrophilic head and a hydrophobic tail and can therefore act as a surfactant. For non-ionic polymer-surfactant mixtures there is usually no strong effective attraction between the compounds, therefore, phase separation is segregative, meaning that two phases are build where one substance is enriched in each phase.⁴¹ According to literature, polymer-surfactant systems show a few similarities to polymer-polymer systems regarding segregative phase separation.⁴² Furthermore, the transient bilayer theory is partially applicable to certain mixtures of small molecules and polymers. Vertical stratification during spin casting is a known effect in organic thin-film transistor (OFT) production, which is utilized to manufacture two layered systems.⁴³ Still, SA is much smaller than a polymer and therefore the resulting structures differ from those observed in binary polymer systems and surface enrichment processes, accompanied by agglomerate formation, play a role. The cellulose:SA blend films at 1:1 and 1:3 ratios display similar morphologies and RMS roughness (Figure 4), whereas the surface of the blend at the ratio of 3:1 looks completely different. This trend is observed in the SFE as well, since the SFE

of the cellulose:SA blend ratios of 1:1 ($61.4 \pm 0.2 \text{ mJ}\cdot\text{m}^{-2}$) and 1:3 ($61.8 \pm 0.3 \text{ mJ}\cdot\text{m}^{-2}$) are higher compared to the ratio of 3:1 ($42.2 \pm 0.1 \text{ mJ}\cdot\text{m}^{-2}$). The SFE of the cellulose:SA blend at the ratio of 3:1 is approximately in between values of pure cellulose ($62.8 \pm 0.6 \text{ mJ}\cdot\text{m}^{-2}$) and pure SA ($21.2 \pm 0.3 \text{ mJ}\cdot\text{m}^{-2}$) films. Since the films of cellulose:SA at ratios of 1:1 and 1:3 exhibit low RMS roughness, the SFE can be attributed solely to the influence of the functional groups present at the surface. High roughness and inhomogeneity is observed in the case of the ratio of 3:1, which affects the contact angle and concomitantly the SFE. The orientation of SA might play an important role too, since either the hydrophilic carboxyl head groups or the hydrophobic tails are able to point to the air-polymer interface.

Treatment with CHCl_3 was performed to selectively remove the SA phase and thus assign the domains. As expected, the micron sized platelets ($2.6 \pm 1.1 \text{ }\mu\text{m}$) present on the surface of the cellulose:SA blend at the ratio 3:1 stem from the SA phase. The spots where SA platelets were present prior to solvent treatment were still traceable afterwards. Additionally, small holes were found inside the CHCl_3 treated film similar to the ones observed at the other ratios. The size of those holes (ranging from 30 to 90 nm) increases with increasing SA content in the blend. These findings basically indicate the same type of morphology for all films. Nevertheless, it is still unclear why huge aggregates arise during spin casting of the films with the lowest SA content.

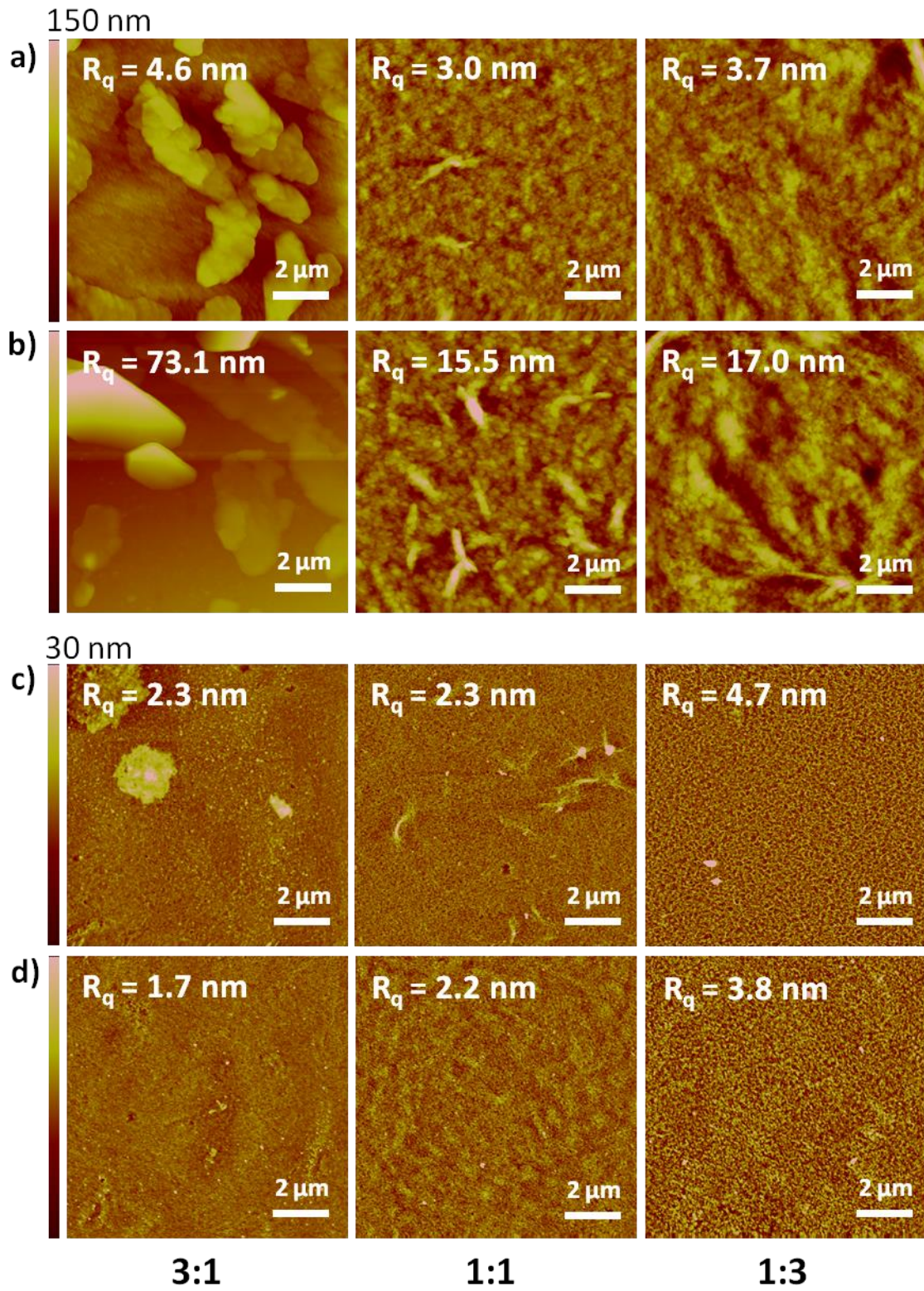


Figure 4. Atomic force microscopy height images and corresponding RMS roughness (R_q) of TMSC:SA blend films spin coated at different ratios before (a) and after (b) exposure to HCl vapors, as well as after treatment with (c) CHCl_3 and (d) BSA (picture size $10 \times 10 \mu\text{m}^2$).

Table 2. Area of cellulose, CSE and SA phases occurring in the blend films at different ratios calculated from atomic force microscopy data.

cellulose:CSE	cellulose [%]	CSE [%]	cellulose:SA	cellulose [%]	SA [%]
3:1	28	72	3:1	57	43
1:1	20	80	1:1	54	46
1:3	11	89	1:3	57	43

Protein interaction at blend surfaces. The interaction of the investigated surfaces and proteins was monitored by multi-parameter surface plasmon resonance spectroscopy (MP-SPR) at the example of *bovine serum albumin* (BSA), which is a commonly used marker for nonspecific protein adsorption. The real-time adsorption behavior of BSA toward the cellulose:CSE blends is depicted in Figure 5. An overshoot effect, presumably caused by reorganization of the protein molecules on the surface⁴⁴, and fast adsorption kinetics, represented by the steep slope of the sensogram, is observed for all surfaces. The extent of the overshoot effect is more pronounced for pure CSE and the cellulose:CSE blend at the ratio of 1:3 featuring lower SFE compared to the other films. The hydrophobicity of the film surface seems to influence BSA adsorption. Cellulose exhibits low protein adsorption ($0.4 \pm 0.1 \text{ mg}\cdot\text{m}^{-2}$), while hydrophobized cellulose displays a value as twice as high ($0.8 \pm 0.1 \text{ mg}\cdot\text{m}^{-2}$). Protein adsorption of the cellulose:CSE blend at the ratio of 1:3 ($0.7 \pm 0.1 \text{ mg}\cdot\text{m}^{-2}$) is comparable to pure CSE. In

contrast, cellulose:CSE blends at ratios of 3:1 and 1:1 exhibit even lower protein adsorption than cellulose. This phenomenon can be probably traced back to the morphology of the blend films since the SFE do not exhibit significant differences. The area of CSE (see Table 2) is approximately the same for all blend ratios and therefore preferential adsorption onto either one or the other blend compound is not the reason for minimized BSA deposition. According to literature, BSA forms island-like structures during adsorption which fuse into patches until a complete monolayer coverage is realized on the surface.⁴⁵ In the case of cellulose:CSE blends at the ratios of 3:1 and 1:1, the growth mechanism of the BSA layer is interrupted by the cellulose domains, whereas at the ratio of 1:3, the CSE phase is only perforated by very small cellulose parts, therefore protein adsorption is not influenced to a high extent. Interestingly, in blends composed of cellulose and lignin fatty acid ester, the latter acts as a sacrificial compound, which is removed upon rinsing with protein solution.²⁷ Maybe the lower mass (few kDa) of the lignin fatty acid ester compared to the CSE (>50 kDa) is responsible for this behavior.

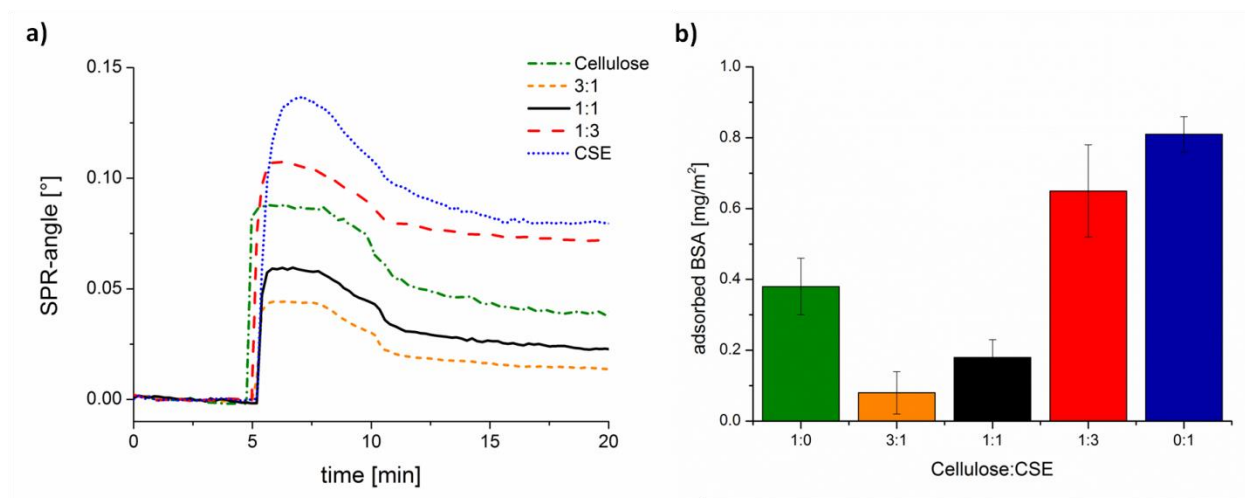


Figure 5. Sensograms (a) measured at 785 nm during adsorption of BSA onto blend films of cellulose and CSE at different ratios and corresponding amounts of adsorbed protein (b) calculated from change in SPR-angle.

Initially, the MP-SPR experiments for the cellulose:SA blends were performed in the same fashion as for the ones containing CSE. We were surprised to observe a strong decrease in SPR angle upon injection of protein solution into the flow cell indicating desorption of material for all blends containing SA. Therefore, the rinsing step with protein solution was prolonged until a stable signal was detected (Figure 6a), meaning that nothing was removed from the surface anymore.

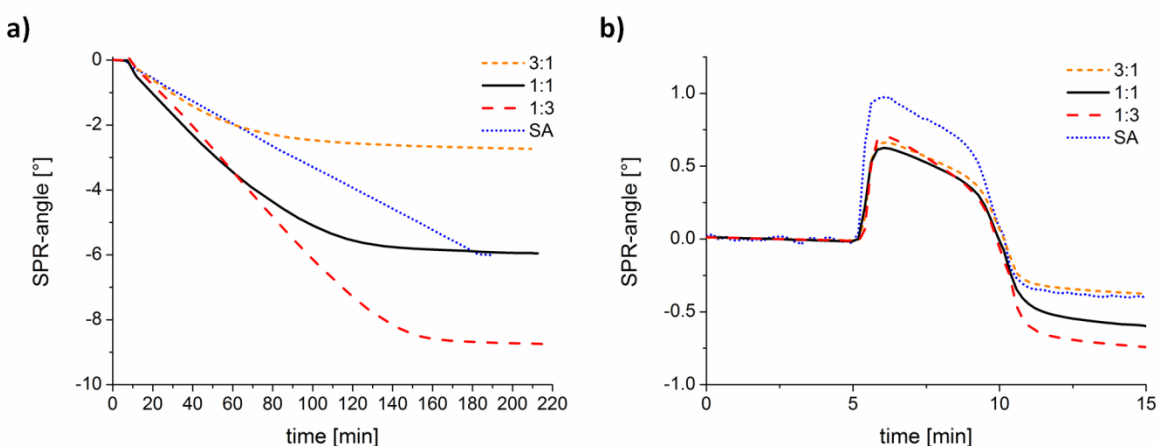


Figure 6. Sensograms measured at 785 nm during rinsing with (a) $1 \text{ mg}\cdot\text{ml}^{-1}$ BSA until reaching a steady signal and (b) $50 \text{ mg}\cdot\text{ml}^{-1}$ BSA for a period of 5 min of cellulose:SA blend films at different ratios.

Afterwards, AFM images were recorded and compared to images of surfaces, which were immersed in CHCl_3 in order to remove SA. AFM investigations after both treatments displayed very similar results (Figure 4) indicating that the rinsing procedure with BSA leads to the removal of SA from the cellulose matrix. This originates from the ability of BSA to build

complexes with fatty acids⁴⁶⁻⁴⁸, which are then rinsed away by the flow. The higher the SA content of the blend, the more material is removed resulting in smaller SPR angles. The period until the entire SA is depleted from the surfaces takes longer for blends containing a higher amount of SA (80 min, 130 min, 150 min, for cellulose:SA 3:1, 1:1 and 1:3, respectively). The experiment for pure SA was stopped after 180 min, since it clearly showed the slowest SA removal. In terms of kinetics, the slope of the curve during rinsing with protein is steeper, indicating faster desorption, for blends with higher SA content.

Furthermore, the material was tested at higher BSA concentrations to evaluate the borders of this approach. The experiments were conducted at a BSA concentration of 50 mg·ml⁻¹ corresponding to the concentration of human serum proteins.⁴⁹ The sensograms (Figure 6b) indicate an initial increase in SPR angle correlating to protein adsorption; however, after a maximum of two minutes the signal decreases again. This initial adsorption can be attributed to the BSA deposition onto the cellulose parts of the blends, which is already accompanied by desorption of SA. After a period of 5 min, the surfaces were rinsed with buffer leading to a constant signal, which is below the SPR angle value detected before adsorption for all surfaces. One might argue that the removal of material is simply caused by the forces induced by rinsing, however, when rinsing with buffer without protein the signal is constant. BSA features the same adsorption behavior towards all blends in the beginning of the experiment, except for the pure SA surface, where BSA shows higher affinity. As for the removal of SA, the same trends as noticed for the experiments performed at lower BSA concentration was observed. In both experiments, the pure SA film is less prone to the BSA treatment. Although all cellulose:SA blends depict similar area ratios for the two phases (Table 2), the blends with ratios of 1:3 and 3:1 are rather flat, whereas the films at the ratio of 3:1 and the pure SA films show increased

RMS roughness. The presence of platelets on these surfaces results in higher SA surface area than for the other films. Regardless, flat surfaces are apparently better accessible to BSA and the resulting BSA-SA complex diffuses faster from those surfaces. The BSA-SA complex sticks better to the surfaces where the SA residue is embedded in a large SA phase, due to cohesion, rather than in the case where SA is surrounded by cellulose. The BSA-SA complex is easier released from the blends with small SA domains, i.e. cellulose:SA at ratios of 1:3 and 1:1.

Moreover, protein interaction at the investigated blend surfaces was monitored by high speed AFM to show the process in real-time and to gain better insight into the mechanisms (Figure S7-S9, †ESI). However, when conducting the experiments, the SA domains were scratched by the cantilever movement due to the soft nature of the SA residue. In terms of cellulose:CSE blends, protein adsorption capacity was too low to detect adsorbed proteins. Hardly any change was observed in the overall morphology.

CONCLUSION

In summary, the influence of fatty acids and fatty acid esters on nonspecific protein adsorption on cellulosic surfaces was investigated at 1 and 50 mg ml⁻¹ BSA. When free fatty acids were present in the films, nonspecific protein adsorption was prevented by complexation of BSA with the fatty acid, finally leading to the removal of the fatty acid from the films. This sacrificial behavior is slightly dependent on the accessibility of the surfaces to BSA, i.e. better accessibility leads to more pronounced complexation. In contrast, the covalently bound fatty acid in CSE affects the films in a different way. Here, complexation of the BSA concomitant with a sacrificial mechanism was not observed. Instead, the morphology of the blends and the surface free energies seem to influence the nonspecific adsorption of proteins since they avoid the formation of monolayer like coverage of BSA molecules. For pure CSE for instance, higher BSA

adsorption was observed compared to cellulose, whereas for the 3:1 blend (cellulose:CSE), adsorption was reduced by a factor of two compared to pure cellulose.

In conclusion, mixing cellulose with cellulose fatty acid ester can be utilized to tune protein adsorption by choosing the added amount of hydrophobic compound. Surfaces resistant to protein adsorption can be manufactured by blending cellulose with free fatty acids. In both cases, we were able to attain insights into the interactions occurring at hydrophobized cellulosic surfaces.

ASSOCIATED CONTENT

Supporting Information. Supplementary ATR-IR spectra and AFM images, contact angle data and thickness values.

AUTHOR INFORMATION

Notes

The authors declare no competing financial interests.

ACKNOWLEDGMENT

Part of the work was supported by the People Programme (Marie Curie Actions – Career Integration Grants) of the European Union’s Seventh Framework Programme (FP7/2007-2013) under REA grant agreement n°618158 (PhotoPattToCell).

REFERENCES

- (1) Berg, J. M.; Tymoczko, J. L.; Stryer, L. *Fatty Acid Metabolism*. 5th ed.; W. H. Freeman: New York, 2002.
- (2) Johansson, I.; Svensson, M. Surfactants based on fatty acids and other natural hydrophobes. *Curr. Opin. Colloid Interface Sci.* **2001**, *6*, 178-188.
- (3) Gunstone, F. D. *Fatty Acid and Lipid Chemistry*. 1st ed.; Blackie: London, UK, 1996.
- (4) Thielemans, W.; Wool, R. P. Lignin Esters for Use in Unsaturated Thermosets: Lignin Modification and Solubility Modeling. *Biomacromolecules* **2005**, *6*, 1895-1905.
- (5) Edgar, K. J. Cellulose esters in drug delivery. *Cellulose* **2007**, *14*, 49-64.
- (6) Meng, X.; Roy Choudhury, S.; Edgar, K. J. Multifunctional cellulose esters by olefin cross-metathesis and thiol-Michael addition. *Polym. Chem.* **2016**, *7*, 3848-3856.
- (7) Liu, S.; Liu, J.; Esker, A. R.; Edgar, K. J. An Efficient, Regioselective Pathway to Cationic and Zwitterionic N-Heterocyclic Cellulose Ionomers. *Biomacromolecules* **2016**, *17*, 503-513.
- (8) Edgar, K. J.; Pecorini, T. J.; Glasser, W. G. Long-Chain Cellulose Esters : Preparation , Properties , and Perspective. In *Cellulose Derivatives*, American Chemical Society: Washington, 1998; pp 38-60.
- (9) Fox, S. C.; Li, B.; Xu, D.; Edgar, K. J. Regioselective esterification and etherification of cellulose: A review. *Biomacromolecules* **2011**, *12*, 1956-1972.
- (10) Wang, P.; Tao, B. Y. Synthesis and characterization of long-chain fatty acid cellulose ester (FACE). *J. Appl. Polym. Sci.* **1994**, *52*, 755-761.

- (11) Peydecastaing, J.; Girardeau, S.; Vaca-Garcia, C.; Borredon, M. E. Long chain cellulose esters with very low DS obtained with non-acidic catalysts. *Cellulose* **2006**, *13*, 95-103.
- (12) Huang, F.; Wu, X.; Yu, Y.; Lu, Y.; Chen, Q. Acylation of cellulose nanocrystals with acids/trifluoroacetic anhydride and properties of films from esters of CNCs. *Carbohydr. Polym.* **2017**, *155*, 525-534.
- (13) Granström, M.; Kettunen née Pääkkö, M.; Jin, H.; Kolehmainen, E.; Kilpeläinen, I.; Ikkala, O. Highly water repellent aerogels based on cellulose stearoyl esters. *Polym. Chem.* **2011**, *2*, 1789.
- (14) Vuoti, S.; Talja, R.; Johansson, L. S.; Heikkinen, H.; Tammelin, T. Solvent impact on esterification and film formation ability of nanofibrillated cellulose. *Cellulose* **2013**, *20*, 2359-2370.
- (15) Freire, C. S. R.; Silvestre, A. J. D.; Pascoal Neto, C.; Belgacem, M. N.; Gandini, A. Controlled heterogeneous modification of cellulose fibers with fatty acids: Effect of reaction conditions on the extent of esterification and fiber properties. *J. Appl. Polym. Sci.* **2006**, *100*, 1093-1102.
- (16) Edgar, K. J.; Buchanan, C. M.; Debenham, J. S.; Rundquist, P. A.; Seiler, B. D.; Shelton, M. C.; Tindall, D. Advances in cellulose ester performance and application. *Prog. Polym. Sci.* **2001**, *26*, 1605-1688.
- (17) Bras, J.; Vaca-Garcia, C.; Borredon, M. E.; Glasser, W. Oxygen and water vapor permeability of fully substituted long chain cellulose esters (LCCE). *Cellulose* **2007**, *14*, 367-374.

- (18) Kulomaa, T.; Matikainen, J.; Karhunen, P.; Heikkilä, M.; Fiskari, J.; Kilpeläinen, I. Cellulose fatty acid esters as sustainable film materials – effect of side chain structure on barrier and mechanical properties. *RSC Adv.* **2015**, *5*, 80702-80708.
- (19) Willberg-Keyriläinen, P.; Talja, R.; Asikainen, S.; Harlin, A.; Ropponen, J. The effect of cellulose molar mass on the properties of palmitate esters. *Carbohydr. Polym.* **2016**, *151*, 988-995.
- (20) Krasnou, I.; Tarasova, E.; Märtson, T.; Krumme, A. Thermoplastic cellulose stearate and cellulose laurate: Melt rheology, processing and application potential. *Int. Polym. Proc.* **2015**, *30*, 210-216.
- (21) Krasnou, I.; Gårdebjer, S.; Tarasova, E.; Larsson, A.; Westman, G.; Krumme, A. Permeability of water and oleic acid in composite films of phase separated polypropylene and cellulose stearate blends. *Carbohydr. Polym.* **2016**, *152*, 450-458.
- (22) Tang, L.; Eaton, J. W. Fibrin(ogen) mediates acute inflammatory responses to biomaterials. *J. Exp. Med.* **1993**, *178*, 2147-2156.
- (23) Kalasin, S.; Santore, M. M. Non-specific adhesion on biomaterial surfaces driven by small amounts of protein adsorption. *Colloids Surf., B* **2009**, *73*, 229-236.
- (24) Vogel, V.; Baneyx, G. The tissue engineering puzzle: a molecular perspective. *Ann. Rev. Biomed. Eng.* **2003**, *5*, 441-463.
- (25) Mohan, T.; Niegellhell, K.; Nagaraj, C.; Reishofer, D.; Spirk, S.; Olschewski, A.; Stana Kleinschek, K.; Kargl, R. J. Interaction of tissue engineering substrates with serum proteins and its influence on human primary endothelial cells. *Biomacromolecules* **2017**, *18*, 413-421.

- (26) Taajamaa, L.; Rojas, O. J.; Laine, J.; Yliniemi, K.; Kontturi, E. Protein-assisted 2D assembly of gold nanoparticles on a polysaccharide surface. *Chem. Commun.* **2013**, *49*, 1318-1320.
- (27) Strasser, S.; Niegelhell, K.; Kaschowitz, M.; Markus, S.; Kargl, R.; Stana-Kleinschek, K.; Slugovc, C.; Mohan, T.; Spirk, S. Exploring Nonspecific Protein Adsorption on Lignocellulosic Amphiphilic Bicomponent Films. *Biomacromolecules* **2016**, *17*, 1083-1092.
- (28) Niegelhell, K.; Süßenbacher, M.; Jammerneegg, K.; Ganner, T.; Schwendenwein, D.; Schwab, H.; Stelzer, F.; Plank, H.; Spirk, S. Enzymes as Biodevelopers for Nano- and Micropatterned Bicomponent Biopolymer Thin Films. *Biomacromolecules* **2016**, *17*, 3743-3749.
- (29) Zhang, K.; Geissler, A.; Standhardt, M.; Mehlhase, S.; Gallei, M.; Chen, L.; Marie Thiele, C. Moisture-responsive films of cellulose stearyl esters showing reversible shape transitions. *Sci. Rep.* **2015**, *5*, 11011.
- (30) Kontturi, E.; Thüne, P. C.; Niemantsverdriet, J. W. Cellulose model surfaces-simplified preparation by spin coating and characterization by X-ray photoelectron spectroscopy, infrared spectroscopy, and atomic force microscopy. *Langmuir* **2003**, *19*, 5735-5741.
- (31) Mohan, T.; Kargl, R.; Doliška, A.; Vesel, A.; Köstler, S.; Ribitsch, V.; Stana-Kleinschek, K. Wettability and surface composition of partly and fully regenerated cellulose thin films from trimethylsilyl cellulose. *J. Colloid Interface Sci.* **2011**, *358*, 604-610.
- (32) Owens, D. K.; Wendt, R. C. Estimation of the surface free energy of polymers. *J. Appl. Polym. Sci.* **1969**, *13*, 1741-1747.
- (33) Rabel, W. Einige Aspekte der Benetzungstheorie und ihre Anwendung auf die Untersuchung und Veränderung der Oberflächeneigenschaften von Polymeren. *Farbe Lack* **1971**, *77*, 997-1005.

- (34) Kaelble, D. H. Dispersion-Polar Surface Tension Properties of Organic Solids. *J. Adhes.* **1970**, *2*, 66-81.
- (35) De Feijter, J.; Benjamins, J.; Veer, F. Ellipsometry as a tool to study the adsorption behavior of syntetic and biopolymers at the air water interface. *Biopolymers* **1978**, *17*, 1759-1772.
- (36) Robeson, J. L.; Tilton, R. D. Spontaneous Reconfiguration of Adsorbed Lysozyme Layers Observed by Total Internal Reflection Fluorescence with a pH-Sensitive Fluorophore. *Langmuir* **1996**, *12*, 6104-6113.
- (37) Mohan, T.; Spirk, S.; Kargl, R.; Doliška, A.; Vesel, A.; Salzmann, I.; Resel, R.; Ribitsch, V.; Stana-Kleinschek, K. Exploring the rearrangement of amorphous cellulose model thin films upon heat treatment. *Soft Matter* **2012**, *8*, 9807.
- (38) Heriot, S. Y.; Jones, R. A. L. An interfacial instability in a transient wetting layer leads to lateral phase separation in thin spin-cast polymer-blend films. *Nat. Mat.* **2005**, *4*, 782-786.
- (39) Walheim, S.; Böltau, M.; Mlynek, J.; Krausch, G.; Steiner, U. Structure Formation via Polymer Demixing in Spin-Cast Films. *Macromolecules* **1997**, *30*, 4995-5003.
- (40) Kontturi, E.; Johansson, L.-S.; Laine, J. Cellulose decorated cavities on ultrathin films of PMMA. *Soft Matter* **2009**, *5*, 1786-1788.
- (41) Piculell, L.; Lindman, B. Association and Segregation in Aqueous Polymer/Polymer, Polymer Surfactant, and Surfactant Surfactant Mixtures - Similarities and Differences. *Adv. Colloid Interface Sci.* **1992**, *41*, 149-178.
- (42) Lindman, B.; Khan, A.; Marques, E.; Miguel, G.; Piculell, L. Phase behavior of polymer-surfactant systems in relation to polymer-polymer and surfactant- surfactant mixtures. *Pure Appl. Chem.* **1993**, *65*, 953-958.

- (43) Zhao, K.; Wodo, O.; Ren, D.; Khan, H. U.; Niazi, M. R.; Hu, H.; Abdelsamie, M.; Li, R.; Li, E. Q.; Yu, L.; Yan, B.; Payne, M. M.; Smith, J.; Anthony, J. E.; Anthopoulos, T. D.; Thoroddsen, S. T.; Ganapathysubramanian, B.; Amassian, A. Vertical Phase Separation in Small Molecule:Polymer Blend Organic Thin Film Transistors Can Be Dynamically Controlled. *Adv. Funct. Mater.* **2016**, *26*, 1737-1746.
- (44) Rabe, M.; Verdes, D.; Seeger, S. Understanding protein adsorption phenomena at solid surfaces. *Adv. Colloid Interface Sci.* **2011**, *162*, 87-106.
- (45) Wangkam, T.; Yodmongkol, S.; Disrattakit, J.; Sutapun, B.; Amarit, R.; Somboonkaew, A.; Sriksirin, T. Adsorption of bovine serum albumin (BSA) on polystyrene (PS) and its acid copolymer. *Curr. Appl. Phys.* **2012**, *12*, 44-52.
- (46) Cistola, D. P.; Small, D. M.; Hamilton, J. A. Carbon 13 NMR Studies of Saturated Fatty Acids Bound to Bovine Serum Albumin. *J. Biol. Chem.* **1987**, *262*, 10980-10985.
- (47) Choi, J.-K.; Ho, J.; Curry, S.; Qin, D.; Bittman, R.; Hamilton, J. A. Interactions of very long-chain saturated fatty acids with serum albumin. *J. Lipid Res.* **2002**, *43*, 1000-1010.
- (48) Curry, S.; Brick, P.; Franks, N. P. Fatty acid binding to human serum albumin: new insights from crystallographic studies. *Biochim. Biophys. Acta* **1999**, *1441*, 131-140.
- (49) Peters Jr, T. *All About Albumin*. Academic Press: San Diego, 1995.

For Table of Contents Use Only

How Bound and Free Fatty Acids in Cellulose Films Impact Nonspecific Protein Adsorption

Katrin Niegelhell, Michael Süßenbacher, Jürgen Sattelkow, Harald Plank, Yonggui Wang, Kai

Zhang and Stefan Spirk

